Available online at www.sciencedirect.com
ScienceDirect
Remote Sensing of Environment 112 (2008) 19–34
Remote Sensing of Environment
www.elsevier.com/locate/rse

Remote sensing of woody shrub cover in desert grasslands using MISR with a geometric-optical canopy reflectance model

Mark Chopping [a,*], Lihong Su [a], Albert Rango [b], John V. Martonchik [c], Debra P.C. Peters [b], Andrea Laliberte [b]

[a] Earth and Environmental Studies, Montclair State University, Montclair, NJ 07043, USA
[b] USDA, ARS Jornada Experimental Range, Las Cruces, NM 88003, USA
[c] NASA Jet Propulsion Laboratory, Pasadena, CA, 91109, USA

Received 13 November 2005; received in revised form 10 April 2006; accepted 15 April 2006

Abstract

A new method is described for the retrieval of fractional cover of large woody plants (shrubs) at the landscape scale using moderate resolution multi-angle remote sensing data from the Multiangle Imaging SpectroRadiometer (MISR) and a hybrid geometric-optical (GO) canopy reflectance model. Remote sensing from space is the only feasible method for regularly mapping woody shrub cover over large areas, an important application because extensive woody shrub encroachment into former grasslands has been seen in arid and semi-arid grasslands around the world during the last 150 years. The major difficulty in applying GO models in desert grasslands is the spatially dynamic nature of the combined soil and understory background reflectance: the background is important and cannot be modeled as either a Lambertian scatterer or by using a fixed bidirectional reflectance distribution function (BRDF). Candidate predictors of the background BRDF at the Sun-target-MISR angular sampling configurations included the volume scattering kernel weight from a Li–Ross BRDF model; diffuse brightness ($\rho 0$) from the Modified Rahman-Pinty-Verstraete (MRPV) BRDF model; other Li–Ross kernel weights (isotropic, geometric); and MISR near-nadir bidirectional reflectance factors (BRFs) in the blue, green, and near infra-red bands. The best method was multiple regression on the weights of a kernel-driven model and MISR nadir camera blue, green, and near infra-red bidirectional reflectance factors. The results of forward modeling BRFs for a 5.25 km^2 area in the USDA, ARS Jornada Experimental Range using the Simple Geometric Model (SGM) with this background showed good agreement with the MISR data in both shape and magnitude, with only minor spatial discrepancies. The simulations were shown to be accurate in terms of both absolute value and reflectance anisotropy over all 9 MISR views and for a wide range of canopy configurations (r^2=0.78, RMSE=0.013, N=3969). Inversion of the SGM allowed estimation of fractional shrub cover with a root mean square error (RMSE) of 0.03 but a relatively weak correlation (r^2=0.19) with the reference data (shrub cover estimated from high resolution IKONOS panchromatic imagery). The map of retrieved fractional shrub cover was an approximate spatial match to the reference map. Deviations reflect the first-order approximation of the understory BRDF in the MISR viewing plane; errors in the shrub statistics; and the 12 month lag between the two data sets.

Keywords: Canopy reflectance modeling; Multi-angle remote sensing; MISR; BRDF

1. Introduction

Over the last 150 years encroachment of woody shrubs into grasslands has occurred in many arid and semi-arid regions of the world, including the western United States, northern Mexico, southern Africa, South America, New Zealand, and Australia (Peters & Gibbens, 2006). Vegetation in deserts plays an important role in determining regional to global characteristics of the Earth's climate and biogeochemistry: loss of vegetation raises regional albedo and air temperatures and also lowers the infiltration of moisture into the soil, leading to higher runoff losses, greater losses of soil nutrients, and regional desertification. In addition, exposed desert soils are a source of wind-borne dust, which can affect the radiative balance of the planet depending on the mineralogy of the

* Corresponding author.
E-mail address: chopping@pegasus.montclair.edu (M. Chopping).

0034-4257/$ - see front matter © 2007 Published by Elsevier Inc.
doi:10.1016/j.rse.2006.04.023

dust and its persistence in the atmosphere (Harrison et al., 2001). Possible causes of encroachment include increased herbivory and trampling by livestock, increased atmospheric CO_2 preferentially benefiting plants with a C_3 photosynthetic pathway (including woody shrubs), changes in fire management regimes, and changes in climate and seasonality. Other tangible effects include a decrease in the usefulness of the land for herbivory (not necessarily vegetation productivity); changes in C, N, and water cycling; a redistribution of C towards below-ground pools; increases in the fraction of exposed soil and therefore albedo; and changes in the spatial arrangement of vegetation, nutrients and soil resources to a more clumped and patchy distribution (Schlesinger et al., 1990), allowing for enhanced entrainment of dust into the air (Gillette & Pitchford, 2004).

Arid and semi-arid grasslands account for between 33 and 50% of the Earth's surface and are usually very extensive. Inventorying changes in vegetation type is thus impossible to achieve on a regular, repeated basis using ground-based measurements or aerial reconnaissance. Remote sensing from space is the only feasible method for mapping and monitoring the extent and density of woody shrub cover over these remote and inaccessible tracts of land. The most widely used method for assessing green vegetation abundance, photosynthetic activity and biomass–spectral vegetation indices calculated as ratios of red:near infra-red (NIR) reflectance — are not as useful in arid environments as elsewhere since they are based on absorption of red light by leaf pigments and the assumption of a relatively NIR-dark soil. Dryland mineral soils are bright in the NIR rendering such indices less effective (Calvão & Palmeirim, 2004; Ni & Li, 2000; Ray, 1995). Some approaches to remote sensing of vegetation in arid environments have addressed the problem of differing soil color, *e.g.* the Soil-Adjusted Vegetation Index (SAVI; Huete, 1988) and the Modified SAVI (Qi et al., 1994), or treated the canopy–soil complex as divided discretely into "soil background" and "vegetation" components. This approach is not likely to be useful for GO modeling studies in an environment where the canopy is highly discontinuous since GO models are formulated to capture the effects of large-scale canopy elements (trees and/or shrubs) and it is more appropriate to model the background as a combined soil-understory complex (in this paper

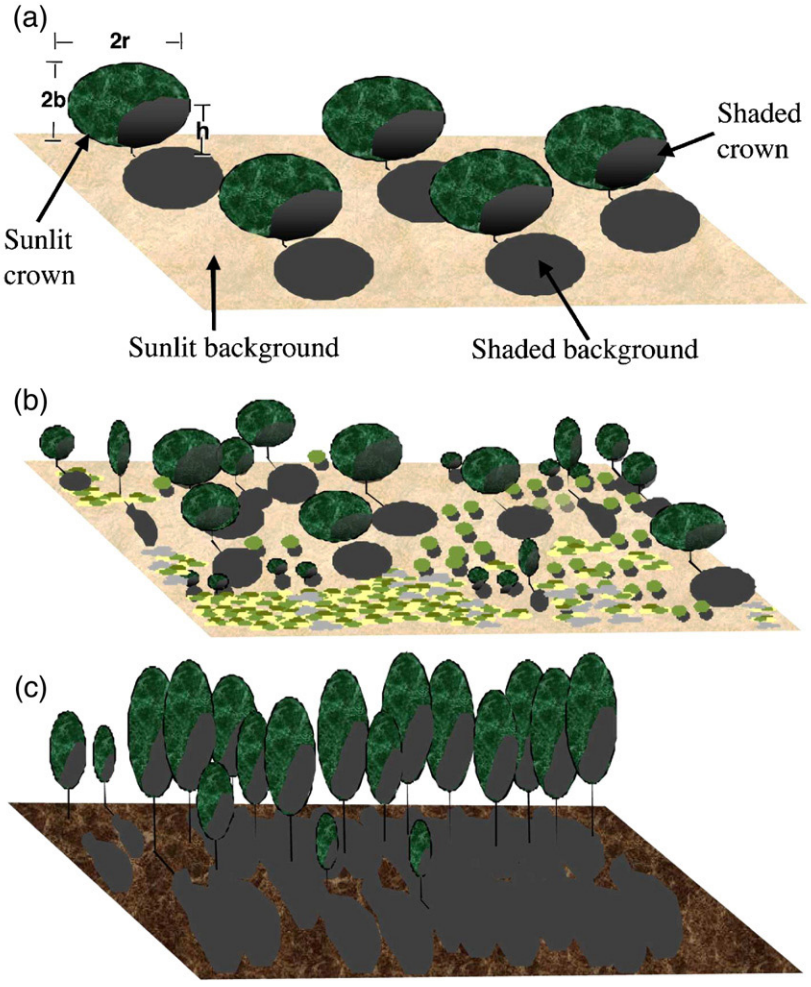

Fig. 1. Geometric-optical model representation of (a) an arid zone shrub-dominated community on a bright, sparse, prominent background (b) an arid zone shrub-dominated community on a bright, prominent, discontinuous background with a spatially-varying BRDF (c) a forested environment: trees over a dark, dense, uniform background.

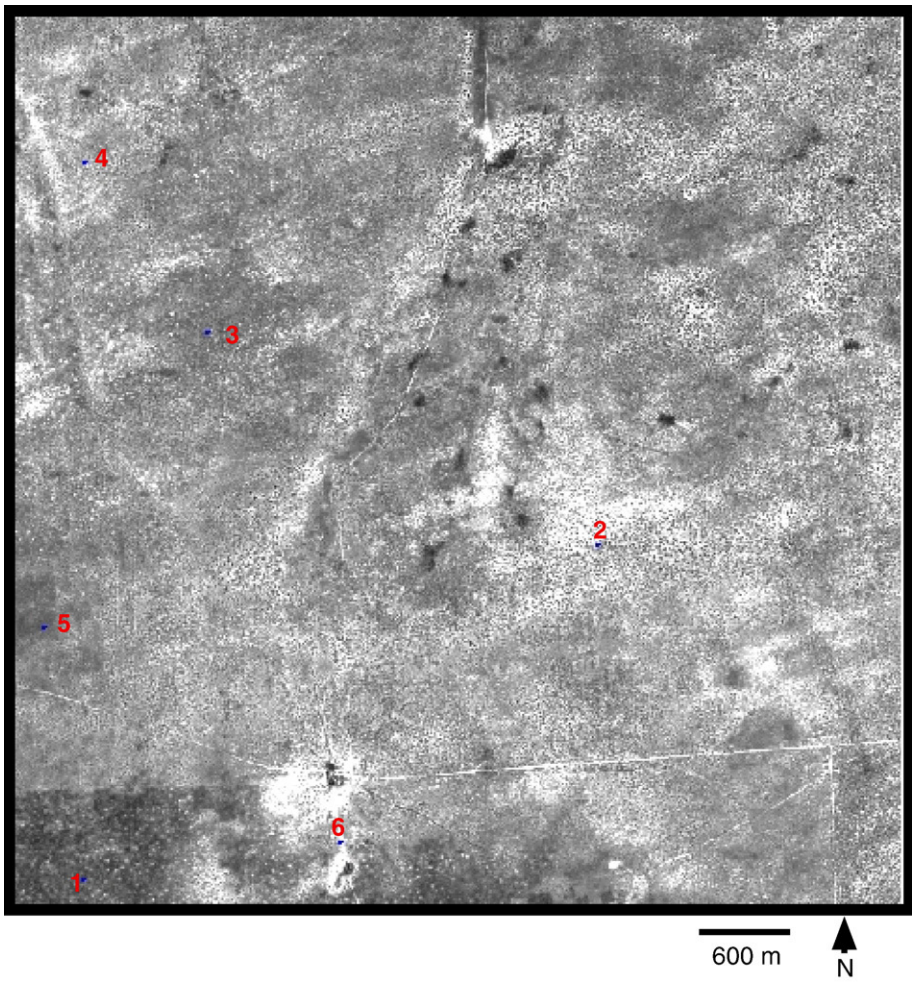

Fig. 2. IKONOS panchromatic image (2 standard deviation stretch) from May 23, 2001 showing the study area and the six sites selected. The West Well is clearly visible in the lower-left quadrant as a dark patch (mostly forbs and annuals) surrounded by a much brighter area of exposed soil, caliche, and larger mesquite shrubs (not visible here). The other large dark areas are swales, depressions which host a dense mixture of shrubs, forbs, annuals and grasses.

"background" is henceforth taken to refer to the combined soil-understory layer; not to soil uniquely). Under this paradigm, soil spectral response is not the most important control on brightness; variations in understory density and composition have an equally or even more profound impact. Similar constraints limit the utility of multi-spectral imaging in the solar spectrum: the reflectance response is highly correlated across most of this wavelength region, limiting the utility of techniques such as spectral unmixing (combining spectral unmixing with GO models is sometimes more appropriate, *cf.* Scarth & Phinn, 2000).

Since grasslands and shrubland canopies exhibit a very high level of spatial heterogeneity (Peters et al., 2006), it has been argued that the most appropriate remote sensing data types for this application are high resolution panchromatic images and aerial photography (Phinn et al., 1996). However, temporal variability is also high in arid regions and initialization, updating and testing of ecological models requires a regular temporal sampling, so it is important to obtain repeat coverage. At a minimum, vegetation type, cover, and condition would be available for important seasonal junctures (end of wet and dry seasons). This cannot be easily achieved using high resolution imagery or aerial photography, in spite of the availability of high quality imagery from the latest generation of commercial imagers with meter or sub-meter ground sampling distances (*e.g.*, IKONOS, QuickBird, Orbview-3). Although these could provide much of the required canopy information over large areas, the cost of data for an extensive mapping effort for a single year would be high and data volumes would be difficult to manage.

Recent developments in remote sensing technology such as imaging spectroscopy that are proving very useful in other environments also have limitations when used in arid environments. It has been shown from first principles that the ability of imaging spectroscopy to provide a spectral vegetation signal is limited when fractional cover is below 0.3 (Okin et al., 2001), although some success has been reported in unmixing of high resolution spectra to estimate the fractional covers of soil, photosynthetic and non-photosynthetic vegetation, albeit over limited areas (Asner et al., 2003). There is thus a role for moderate resolution (~ 250 m), multi-angle, passive, visible to near infrared sensors in this application — not only because these can

Fig. 3. Color aerial photograph from June 2000 over desert grasslands in the Jornada Experimental Range. Note the patchiness of the understory, the grey appearance of the grama grass and the bright exposed soil around some of the larger mesquite shrubs. The photograph also shows the USDA, ARS Cessna Twin 404 piloted by M. R. Davis (photo credit: Scott Bauer, USDA, ARS Photo Unit).

provide regular temporal coverage throughout the year for extensive areas but also because they provide a means of accessing surface information not available to other instruments.

Geometric-optical (GO) models are increasingly used in remote sensing of vegetation as they provide a means of decomposing mixed observations (or "mixed pixels ") into their major components, allowing estimation of canopy parameters such as crown cover, stand density and foliage volume on inversion, using either numerical or lookup table methods (Peddle et al., 2003). Simple GO models treat the surface as an assemblage of geometric objects of equal size, shape and height, evenly distributed within a spatial unit. In these models a tree or shrub crown is represented by a spheroid whose center is located at a specified height above a diffuse scattering (Lambertian) surface (Fig. 1 (a)). These discrete object models were originally developed for use in forested environments (Li & Strahler, 1992) where the soil-understory background is usually darker and thus makes a relatively small contribution to the remotely sensed signal (Fig. 1 (c)); it can often be assumed Lambertian obviating the need to estimate a background bidirectional reflectance distribution function (BRDF) (Ni & Li, 2000), or the relevant part of this. Application of GO models in arid environments with their sparse, discontinuous vegetation and bright soils is much more challenging, as the background cannot be modeled as either Lambertian or by using a fixed BRDF. This is because the cover of understory plant (forbs, annuals, and sub-shrubs) varies spatially and has an important impact on both brightness and reflectance anisotropy (Fig. 1 (b)). As the soil-understory background in these

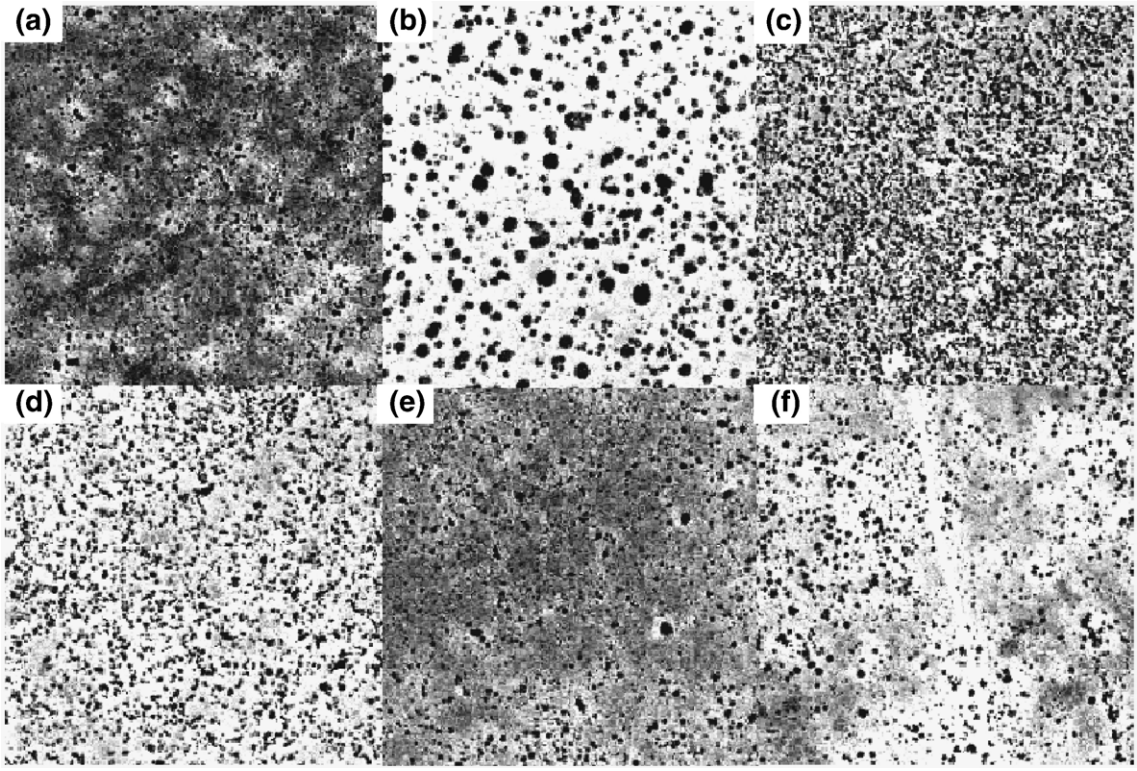

Fig. 4. Variations in canopy configuration in IKONOS 1 m panchromatic image subsets from May 23, 2001 for the six selected 250 m^2 areas corresponding to mapped MISR footprints: (a) dense understory with some shrubs (dark blobs) (b) large shrubs on sand (c) small shrubs on dense understory-1 (d) small shrubs on sparse understory (e) small shrubs on dense understory-2 (f) a mixed area of large shrubs on bright, exposed soil and very dark understory in the vicinity of the West Well. Note that brightness at the scale of a moderate resolution sensor observation is controlled mainly by the understory rather than the large shrubs. Fig. 2 provides the locations of these subsets, where locations 1–6 correspond to (a) through (f), respectively.

environments accounts for a large proportion of the sensor's instantaneous field-of-view (usually >0.7, where background is defined structurally as exposed soil and understory), and since shrubs occur in both grass-dominated and shrub-dominated zones, accurate estimates of shrub cover and other canopy parameters cannot be made without adequate specification of the background contribution. Isolating the signal of the soil-understory complex is thus critical and an important hindrance to the use of GO models in estimating shrub cover in arid environments. Its impact can be appreciated qualitatively through examination of variations in brightness and composition in extensive views of very high resolution panchromatic imagery (Fig. 2), color aerial photography (Fig. 3) and closer views of panchromatic imagery (Fig. 4). The six locations shown in Fig. 4 were chosen to represent widely contrasting upper canopy/soil-understory conditions, ranging from sparse shrubs on a dense understory, through transition zones where shrub invasion has almost completely removed grasses, to stands of very large and old mesquite on very sparse and bright backgrounds.

Although GO models have been shown to perform reasonably well in plot-level studies in desert grasslands (Chopping et al., 2003, 2004a; Franklin & Turner, 1992; Ni & Li, 2000), they have yet to provide canopy parameter maps which are straightforward in their interpretation (Chopping

Table 1
Canopy and reflectance characteristics of six test sites

Site description (shrubs/understory)	Fractional cover	Number density	Radius (m)	Li–Ross kernel weights				MISR An camera BRF			
				Iso	Geo	Vol	RMSE	Blue	Green	Red	NIR
Few small/dense	0.12	0.021	1.38	0.27	0.04	0.01	0.005	0.09	0.15	0.24	0.31
Few large/sparse	0.11	0.008	2.05	0.29	0.03	0.00	0.007	0.08	0.16	0.27	0.36
Many small/dense1	0.21	0.022	1.73	0.27	0.04	0.00	0.005	0.08	0.16	0.25	0.33
Many small/sparse	0.12	0.017	1.47	0.29	0.04	0.00	0.005	0.09	0.16	0.27	0.35
Many small/dense2	0.08	0.014	1.34	0.28	0.04	0.01	0.007	0.09	0.16	0.25	0.32
Variable/variable	0.07	0.013	1.37	0.29	0.05	0.01	0.007	0.09	0.16	0.26	0.34

Note: cover estimates were derived from 1 m panchromatic IKONOS imagery. Radius is the mean over all shrubs within each 250 m^2 area. Li–Ross kernel weights were derived using the LiSparse and RossThin reciprocal kernels.

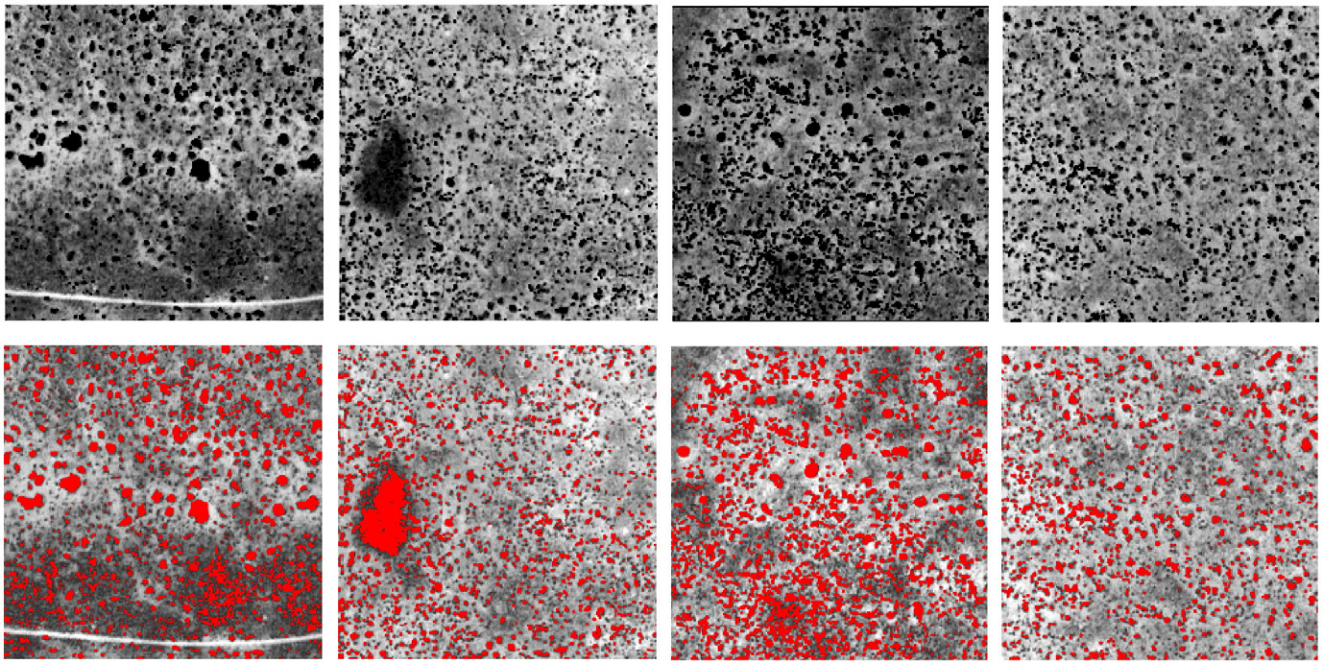

Fig. 5. Top: 250 m^2 IKONOS 1 m panchromatic image subsets corresponding to mapped MISR data. Bottom: thresholded to obtain mean shrub density, radius, and fractional cover used in forward modeling and as reference data.

et al., 2003, 2004b,c,d) and no published studies have demonstrated their usefulness at landscape scales in arid environments. We suggest that this is owing to the need to estimate a spatially dynamic background BRDF, or at least the subset of the BRDF that corresponds to a particular sensor's angular sampling. We investigated a new method for isolating the signal of the combined soil-understory complex using MISR data, so that upper canopy parameters can be retrieved.

2. Method

2.1. Study area

Our studies were conducted in the USDA, ARS Jornada Experimental Range (the Jornada), which is located about 37 km north of Las Cruces, New Mexico (32.5°N, 106.8°W), in the northern part of the Chihuahuan Desert between the Rio Grande floodplain on the west and the San Andres mountains on the east. The Jornada is located at the southern end of a hydrologically closed basin and is characterized by a complex system of alluvial fans and ephemeral stream channels and playa lakes. Much of the basin is dominated by coarse-textured aeolian and fluvial sediments from the Rio Grande river. Mean elevation is about 1350 m. Climate is arid to semi-arid: long-term (1915–1995) mean annual precipitation was 245 mm/y (with a standard deviation of 87) and mean monthly temperatures ranged from 3.8 °C in January to 26.1 °C in July. Precipitation follows a monsoonal pattern with >53% of annual rainfall occurring in July–September. Vegetation is classified as desert grassland and plant communities in the Jornada have experienced major shifts in vegetation composition over the past 50–150 years (Gibbens et al., 2005). The most dramatic changes in vegetation and associated ecosystem processes have occurred as a result of a shift in life form due to woody plant encroachment into perennial grasslands (Bahre & Shelton, 1993; Grover & Brad Musick, 1990). Historical records of vegetation change in the Jornada show a progressive loss of semi-arid grasslands dominated by the perennial C_4 grass black grama (*Bouteloua eriopoda*) and an invasion of C_3 desert shrubland species, predominately creosotebush (*Larrea tridentata*) and honey mesquite (*Prosopis glandulosa*) (Buffington & Herbel, 1965). Honey mesquite is now a major dominant on sandy soils where *Gutierrezia sarothrae* (broom snakeweed) and *Yucca elata* (soaptree yucca) are also abundant. This study focuses on an area where honey mesquite is the major invasive species.

2.2. Remotely sensed data

The primary data set used was from the Multiangle Imaging SpectroRadiometer (MISR) flown on NASA's Earth Observing System Terra satellite launched in December 1999 (Diner et al., 1998). MISR provides spectral radiance images in nine along-track view angles by using nine inter-calibrated cameras. The MISR multi-angle images were acquired from a Terra overpass at the end of the dry season (mid-June 2002). This period was chosen as this is the end of the dry season when shrubs are active but grasses are still dormant awaiting summer convective rainfall.

Red band (672 nm) data were used directly in canopy reflectance modeling as these are the only data acquired by MISR at 275 m in all nine cameras: at nadir viewing and at eight

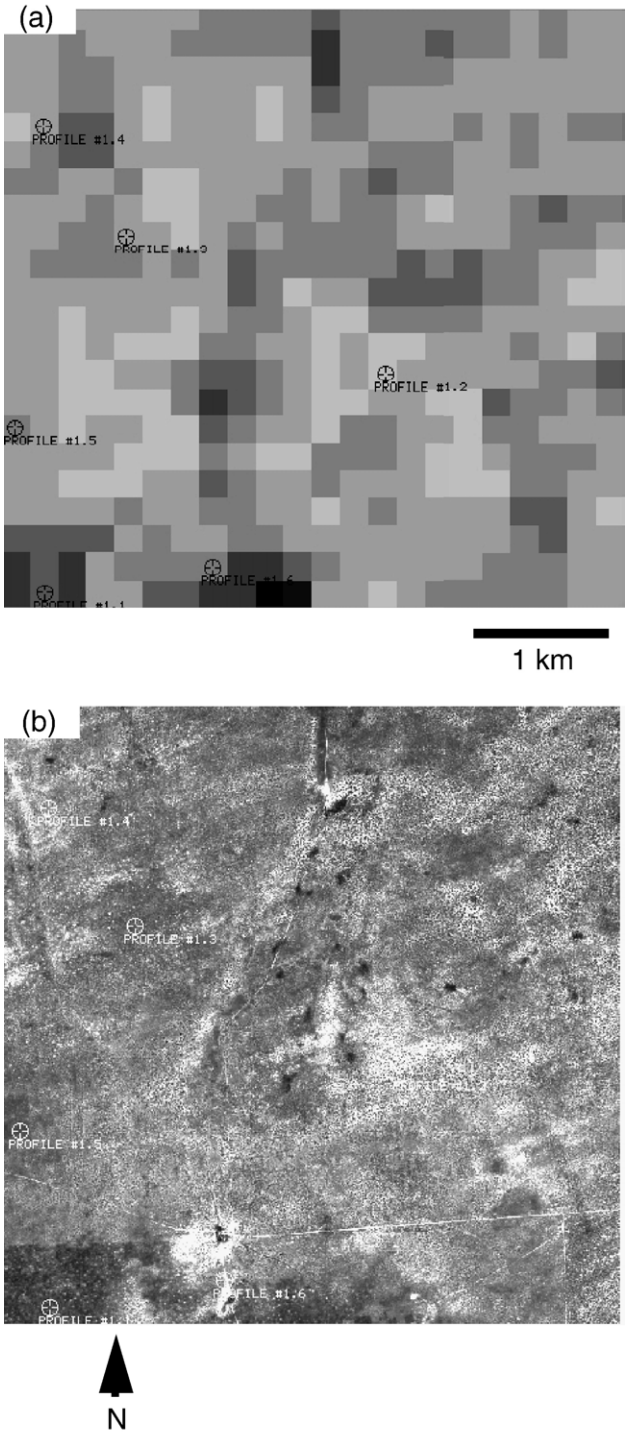

Fig. 6. Correspondence between volume scattering and understory density: (a) volume scattering kernel weight derived from inversion of the isotropic-LiSparse–RossThin model with MISR data *via* AMBRALS. The LUT has been inverted so that higher values are represented by darker shades (b) the corresponding IKONOS panchromatic image. Note the dark areas in the SW quadrant and the dark feature in the center–top of the images.

other viewing angles (26.1°, 45.6°, 60.0°, and 70.5° in the forward and backward directions). The spectral reflectance contrast in the red wavelengths between shrubs and grasses was close to the maximum at this time (in 2002 the drought had not yet broken). GO modeling was restricted to the MISR red band data because in these wavelengths absorption by plant photosynthetic materials and pigments is maximum (and so contrast between soil and shrub crowns is maximum) and the single scattering approximation is more appropriate than in the near-infra-red. This approach is supported by Pinty et al. (2002) which asserts that the wavelength should be chosen to maximize the reflectance/absorption contrasts between vertically clumped elements and the background. Furthermore, Qin and Gerstl (2000) point out that the linear mixture assumption underlying geometric-optical models is more valid for the red than near infra-red wavelengths in arid environments; and BRDF model inversion experiments using numerical methods show that there are generally fewer problems such as trapping at local minima in the red compared to the NIR (Gemmell, 2000). Nadir view blue, green, red, and near infra-red spectral radiance data at 275 m were also used to estimate the corresponding surface reflectance estimates. The data were mapped onto a 250 m UTM grid for use with MODIS reflectance data (not used in this study).

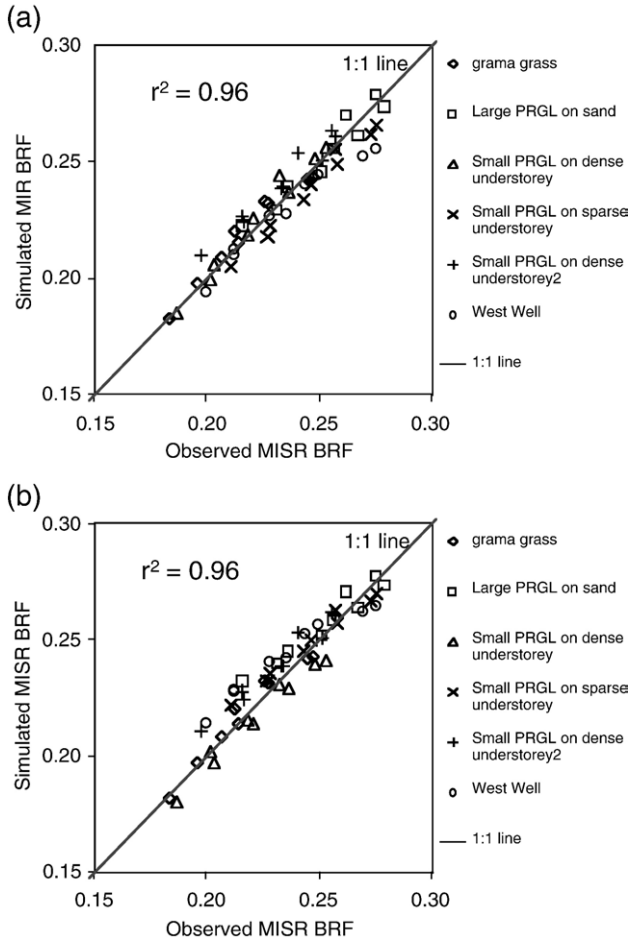

Fig. 7. Scatter plots showing the correspondence between observed and modeled MISR red band BRFs for six sites in the Jornada Experimental Range (a) with the background contribution predicted using volume scattering (b) with the background contribution predicted using diffuse brightness (MRPV $\rho 0$). The absolute RMSE is <0.02 in both cases.

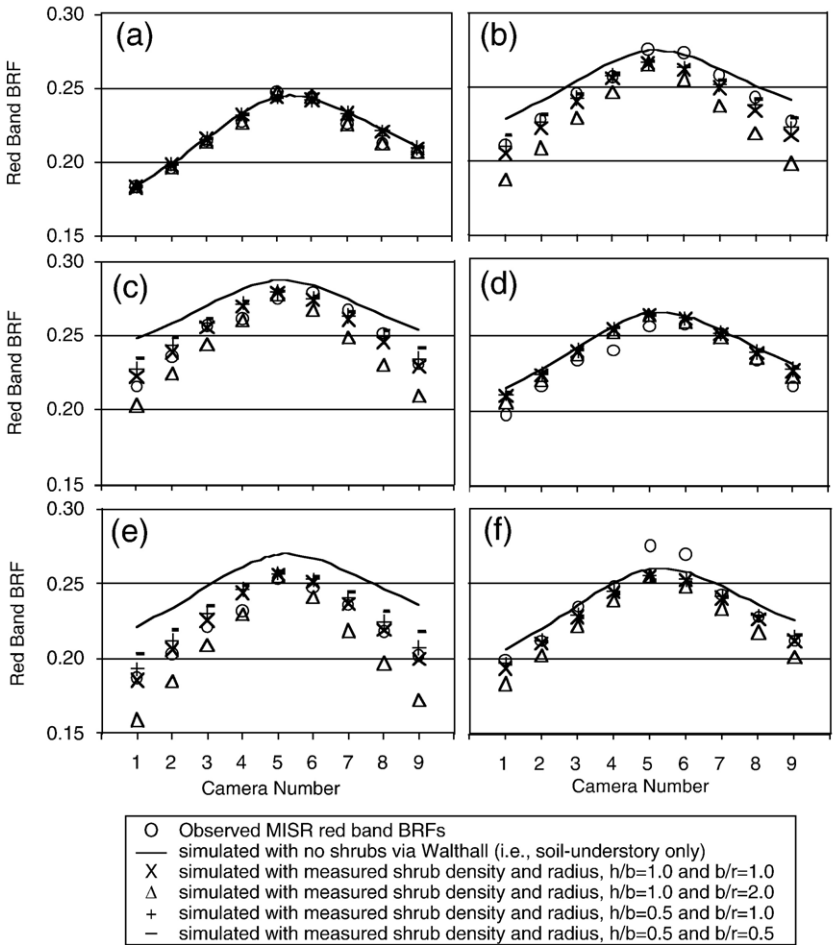

Fig. 8. Simulated (volume scattering only) and observed MISR data for all nine cameras for (a) dense understory with some shrubs (b) small shrubs on sparse understory (c) large shrubs on extremely sparse understory (d) small shrubs on dense understory-2 (e) small shrubs on dense understory-1 (f) a mixed area of large shrubs on bright, exposed soil and very dark understory in the vicinity of the West Well.

Red wavelength surface bidirectional reflectance estimates were retrieved from the MISR MI1B2 Terrain spectral radiance data via corrections for atmospheric scattering and absorption, including MISR aerosol optical depth and estimates of ozone (but not water vapor) using SMAC version 4. Only data from the Da (70° zenith), An (nadir), and Df (70° zenith) cameras were used but from 4 different orbits. The results from SMAC provided values very close to those obtained with 6S v4.1 (r^2>=0.99) over a wide range of surfaces from dark lava flows (two test sites) and large water bodies (Elephant Butte lake) to extremely bright gypsum flats (part of White Sands National Monument) and desert grassland (two test sites with different vegetation density; one in the Sevilleta National Wildlife Refuge and one in the Jornada Experimental Range).

The LiSparse–RossThin kernel-driven model was adjusted against the MISR surface reflectance data set using the **A**lgorithm for **M**odeling **B**idirectional **R**eflectance **A**nisotropies of the **L**and **S**urface (AMBRALS; Wanner et al., 1995) v2.4, providing as output images of estimates of isotropic (diffuse) scattering, geometric scattering, volume scattering, the root mean square error on model fitting (RMSE) and the weight of determination, an indicator of kernel weight sensitivity to the angular sampling (Table 1).

Statistics on large shrub number density and mean radius were extracted from 1 m IKONOS panchromatic imagery for all 250 m^2 locations corresponding to the mapped MISR data using simple thresholding (Fig. 5). The minimum and maximum shrub sizes were set at 1 and 300 (1 m^2) pixels, respectively. Values of shrub cover, number density and mean radius were compared with independent estimates from image segmentation analysis of QuickBird panchromatic imagery and found to be in reasonably good agreement, with an r^2 of 0.6 (Laliberte et al., 2004). These upper canopy parameters were subsequently used in determining the background contribution and in driving the SGM in forward mode for the MISR angular configurations.

2.3. MISR simulations with a canopy reflectance model

A modified version of the simple geometric model (SGM) — a canopy reflectance model which incorporates

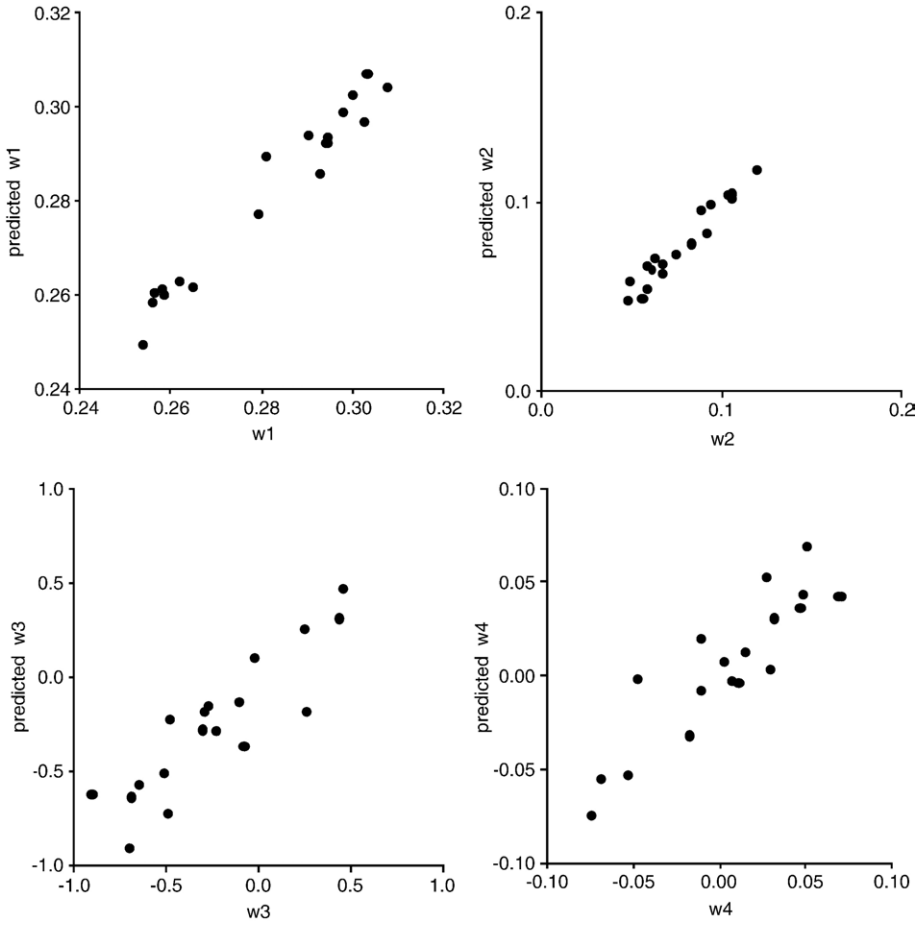

Regression Statistics

	w1	w2	w3	w4
Multiple R	0.98	0.97	0.89	0.89
R Square	0.96	0.94	0.79	0.80
Adj. R Square	0.94	0.91	0.68	0.69
Standard Error	0.00	0.01	0.24	0.02

Fig. 9. Prediction of Walthall model parameters w1–w4 to characterize the background, using isotropic, geometric, and volume scattering kernel weights (LiSparse–RossThin model) and the nadir camera blue, green and near-infra-red BRFs.

geometric optics with a leaf area index-dependent volume scattering term and a spatially dynamic background BRDF — was used here in both forward and inverse modes. The model was developed as a means of exploiting the directional signal embedded in data from multi-angle and off-nadir viewing remote sensing instruments (Chopping et al., 2003, 2004a); its development was motivated by the difficulty in interpreting the parameters of the linear, semi-empirical, kernel-driven models designed for use with wide-swath, across-track, off-nadir sensors such as the AVHRR and MODIS (Wanner et al., 1995), which nevertheless provide excellent global estimates of BRDF and albedo (Schaaf et al., 2005). The SGM was developed by relaxing some important assumptions made by kernel-driven BRDF models, in particular the requirement that the sunlit ground and crown are equally bright. As with kernel-driven models, the SGM assumes potential contributions from both geometric-optical and volume scattering effects and is formulated as (Eq. (1)):

$$\mathrm{BRF} = G_{\mathrm{Walthall}}(\vartheta_i, \vartheta_v, \varphi) \cdot k_{\mathrm{G}}(\vartheta_i, \vartheta_v, \varphi) + C_{\mathrm{Ross}}(\vartheta_i, \vartheta_v, \varphi) \cdot k_{\mathrm{C}}(\vartheta_i, \vartheta_v, \varphi) \quad (1)$$

where BRF is bidirectional reflectance factor; ϑ_i, ϑ_v and φ are the view zenith, solar zenith and relative azimuth angles, respectively; k_{G} and k_{C} are the calculated proportions of sunlit and viewed background and crown, respectively; G_{Walthall} is the calibrated Walthall model (Walthall et al., 1985); and C_{Ross} is the simplified Ross turbid medium approximation for optically-thin or thick plane parallel canopies (Ross, 1981). k_{G} and k_{C} are calculated exactly *via* Boolean geometry for the principal (PP) and cross-principal (CP) planes and approximated away from these (Wanner et al., 1995). The model's parameters are plant number density,

Table 2
Prediction of Walthall model parameters *via* regression (19 observations)

	Regression coefficients			
	w1	w2	w3	w4
Intercept	0.07	0.28	−4.37	0.52
Isotropic	−1.31	1.06	−3.24	−0.55
Geometric	0.50	1.26	12.56	−0.93
Volume scattering	−0.49	−1.01	−67.40	6.85
Blue nadir BRF	−1.40	1.43	56.28	−5.83
Green nadir BRF	2.02	−2.31	−11.02	0.87
NIR nadir BRF	1.09	−0.92	5.58	−0.03
	p-value			
Intercept	0.44	0.04	0.33	0.26
Isotropic	0.27	0.50	0.95	0.92
Geometric	0.45	0.18	0.70	0.78
Volume scattering	0.54	0.37	0.10	0.11
Blue nadir BRF	0.47	0.59	0.55	0.55
Green nadir BRF	0.20	0.27	0.88	0.91
NIR nadir BRF	0.21	0.43	0.89	0.99

Note: regression on LiSparse–RossThin BRDF model kernel weights plus blue, green and near-infrared near-nadir BRFs.

mean crown radius, crown shape (*b*/*r*), crown center height (*h*/*b*), leaf area index (LAI); and the four Walthall model parameters which describe the background BRDF at the relevant geometries. The SGM is not a physical model as the radiative properties of the surface are not handled explicitly; for example, the effects of diffuse irradiance are ignored and all shadows are considered completely dark. However it has provided good results when tested against a radiosity-based model calibrated with detailed ground measurements and against multi-angle observations from the air (Chopping et al., 2003, 2004a). For the simulations effected in this study the model inputs were:

1. The MISR acquisition angles (solar zenith, relative azimuth and view zenith angles; denoted SZA, RAA, and VZA, respectively).
2. Shrub number density and average radius estimated from IKONOS panchromatic imagery at 1 m resolution using simple thresholding.
3. Shrub leaf area index (LAI), which was fixed at 2.08 (White et al., 2000). Note that this is the estimated LAI of a typical shrub, not that of the landscape.
4. The upper canopy shape and height ratios, *h*/*b* and *b*/*r*, where *h* is the average height of the center of crowns above the surface, *b* is the average vertical radius of crowns, and *r* is the average horizontal radius of crown (Fig. 1 (a)).
5. The parameters of the Walthall BRDF model (Walthall et al., 1985), used here to characterize the background BRDF at the relevant geometries. Obtaining the background contribution is the most challenging aspect of GO modeling in arid environments.

2.4. Estimating the soil-understory background contribution

The initial protocol by which the soil-understory background contribution was obtained was the selection of two locations with very contrasting understory densities close to the extremes; set the SGM mean shrub radius and number density using the IKONOS-derived shrub statistics (and fixing *b*/*r* and *h*/*b* at typical values); adjust the four Walthall parameters to minimize the absolute root mean square error with respect to the nine MISR multi-angle observations; and regress the Walthall parameters against some candidate predictor. Initial candidate metrics included nadir view red reflectance, the volume scattering kernel weight from inversion of a linear LiSparse–RossThin model, and the modified Rahman-Pinty-Verstraete *ρ0* (diffuse scattering) parameter (red band). The most straightforward means of estimating the soil-understory background BRDF is to exploit the relationship between cover and nadir reflectance, since the understory is in general a more important control on bare soil exposure than large shrub cover and thus governs brightness. This approach had previously been pursued for model inversion attempts with data from the European Space Agency's Compact High Resolution Imaging Spectrometer (CHRIS) instrument on the Proba satellite (Chopping et al., 2004b). However attempts to use near-nadir or estimated nadir reflectance for this purpose were abandoned because changes in brightness were found to be too severe close to nadir and it was difficult to establish a consistent relationship.

Methods for isolating the soil-understory signal from that of large shrubs (primarily honey mesquite, *P. glandulosa*, denoted PRGL) are not obvious but it was found that a LiSparse–RossThin model volume scattering kernel weight obtained *via* adjustment of the model against MISR data is a better predictor of understory density than nadir reflectance, in spite of its relatively high sensitivity to angular sampling, a behavior which has been recognized in several studies (Chopping, 2000; Hu et al., 1997; Lucht & Lewis, 2000). The relationship between volume scattering and brightness (understory density) can be

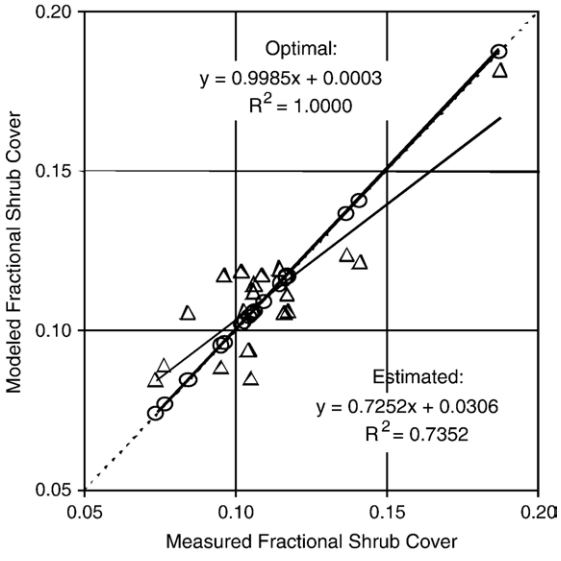

Fig. 10. Impact of using estimated (Δ) over optimal (○) background for 19 cases covering a wide range of shrub number density, mean shrub size, and understory configurations.

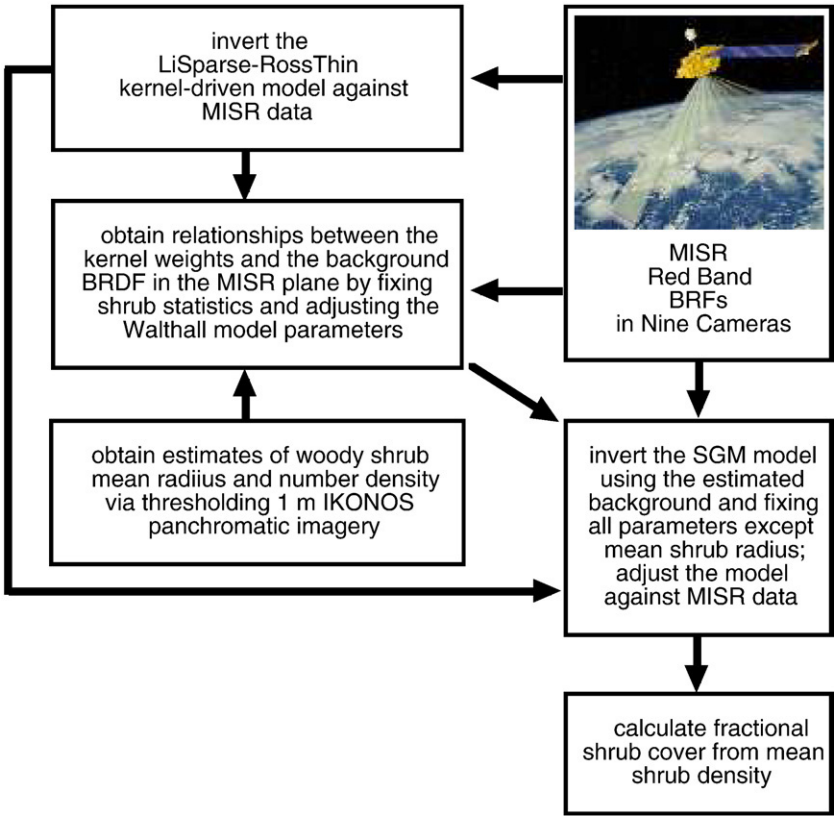

Fig. 11. Flowchart providing an overview of the methods developed for the retrieval of fractional woody shrub cover in desert grasslands using multi-angle red band reflectance data from MISR.

seen by comparing volume scattering kernel weight maps and high resolution IKONOS panchromatic images (Fig. 6). The physical basis for such a relationship is the greater importance of volume scattering when there is a larger number of scattering facets, in this case the leaves of understory plants. The magnitude of the volume scattering parameter is thus thought to reflect foliage density over the area under the sensors instantaneous field-of-view (IFOV), including understory and shrubs, but the density of scatterers is more dependent on the understory than on shrub cover (Fig. 3). The $\rho 0$ (diffuse brightness) parameter retrieved by inversion of the Modified Rahman-Pinty-Verstraete MRPV model was found to perform as well as the volume scattering kernel weight in predicting the background response in simulations for the six sites shown in Fig. 4, with r^2 values of 0.96 and absolute RMSE values <0.02 in both cases (Fig. 7). However, examination of simulated MISR camera profiles for sites with dense understory showed that the estimated background response was too low in both cases; in spite of a fractional shrub cover of 0.12, shrubs had little impact on the modeled signal (Fig. 8(a), (d)), with any realistic setting of the fixed parameters (b/r and h/b, which were varied between 0.25 and 2.00). This is clearly incorrect and points to the likelihood that a single metric holds too little information to accurately predict the parts of the soil-understory background BRDF corresponding to the MISR acquisition geometries.

A more suitable relation was eventually found using multiple regression on the isotropic, geometric and volume scattering kernel weights of the LiSparse–RossThin model (red band) and this was further enhanced by including nadir camera blue, green, and near infra-red BRFs. The regressions were performed using Walthall parameters obtained using the same method as described above for 19 highly contrasting

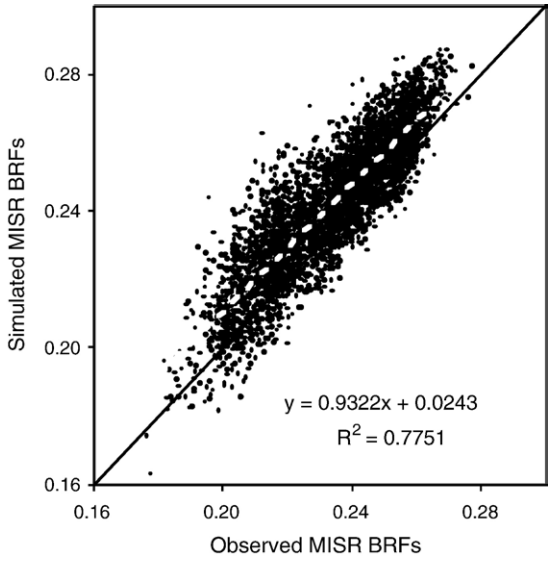

Fig. 12. Simulated *vs* real MISR data, simulations using a soil-understory background estimated from Li–Ross model + blue, green and NIR spectral-nadir BRFs, $N=3969$ (9 views × 441 pixels).

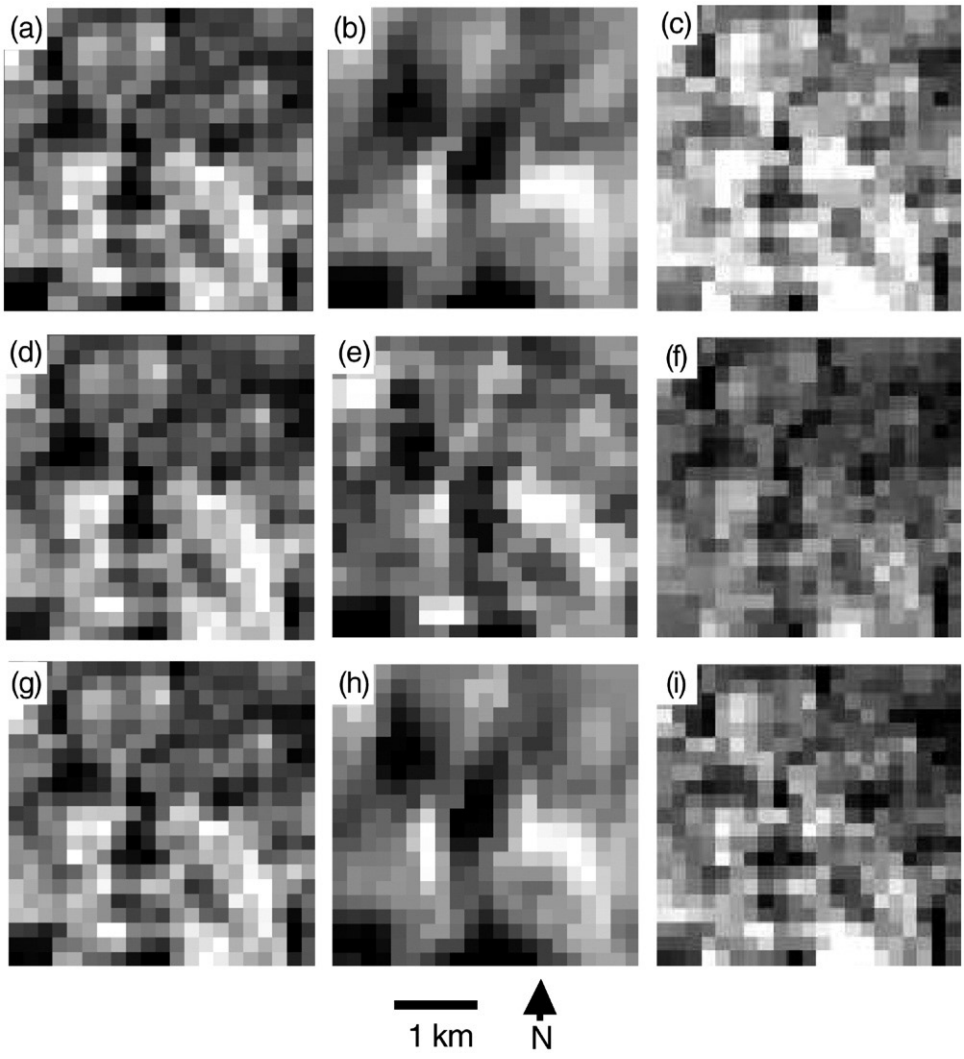

Fig. 13. Simulated and observed MISR red band images. (a) modeled camera 1 (b) MISR camera 1: extreme forward scattering direction (c) camera 1 difference (simulated-observed) (d) modeled camera 5 (d) MISR camera 5: near-nadir (e) modeled camera 5 (f) camera 5 difference (simulated-observed) (g) modeled camera 9 (h) MISR camera 9: extreme backscattering direction (i) camera 9 difference (simulated–observed), scaled between 0.16 and 0.28.

sites: shrub number density and mean radius were set from measured values; leaf area, h/b and b/r were set to typical values of 2.08, 2.0 and 0.2, respectively; and the Walthall model parameters were adjusted to obtain the best match (in terms of absolute RMSE) with MISR observations. Background BRDFs obtained in this way are referred to as "optimal", since they have been obtained to provide the best fit to data. The predicted Walthall parameters obtained for the 19 calibration cases show a reasonable linear relationships to the corresponding optimal parameters (Fig. 9). The regression coefficients retrieved were used to estimate the background BRDF for every location in the study area in both simulations and model inversions. They are given in Table 2, which also demonstrates the importance of the volume scattering kernel weight in predicting the magnitude and — in particular — the shape of the background BRDF at the acquisition geometries of interest. The impact of using an estimated rather than an optimal background is important: the coefficient of determination (r^2) between observed and modeled data for the 19 data sets used in calibration of the regression model is ~ 1.00 if the optimal background is used, declining to 0.74 if it is estimated (Fig. 10).

2.5. MISR scene simulation and model inversion

The SGM was run in forward mode at the acquisition angles of the MISR scene to produce a series of 9 simulated images. Only MISR red band images were simulated because only the red band data are available in all nine views at 275 m. This is very appropriate because in these wavelengths absorption by plant photosynthetic materials and pigments is maximum (and so contrast between soil and vegetation is maximum) and the single scattering approximation is more valid than in the near infra-red. This is supported by Pinty et al. (2002), which asserts that the wavelength should be chosen to maximize the reflectance and absorption contrasts between vertically clumped elements and the background; furthermore, Qin and Gerstl (2000) show that the linear mixture assumption underlying geometric-optical models is

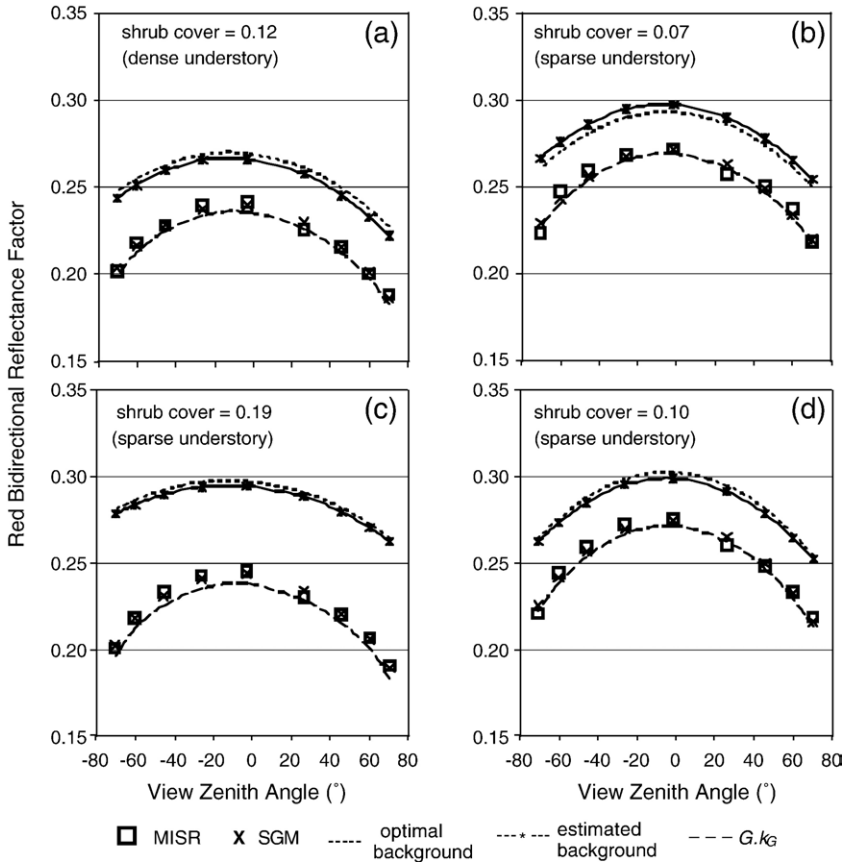

Fig. 14. Typical simulated *vs* real MISR profiles. Simulations used SGM with Walthall from regression of w1–w4 on isotropic, geometric, volume scattering kernel weights and blue, green and NIR nadir BRFs.

more valid for the red than near infra-red wavelengths in arid environments. Simulations were made with fixed values for leaf area, canopy height and shrub shape parameters (LAI, *h*/*b* and *b*/*r* set to 2.08, 2.0 and 0.2, respectively); the previous simulations had shown only small sensitivity to shape and height at these geometries (Fig. 8). Inversion of the SGM was effected for mean shrub radius only, with shrub number density, *b*/*r* and *h*/*b* fixed at

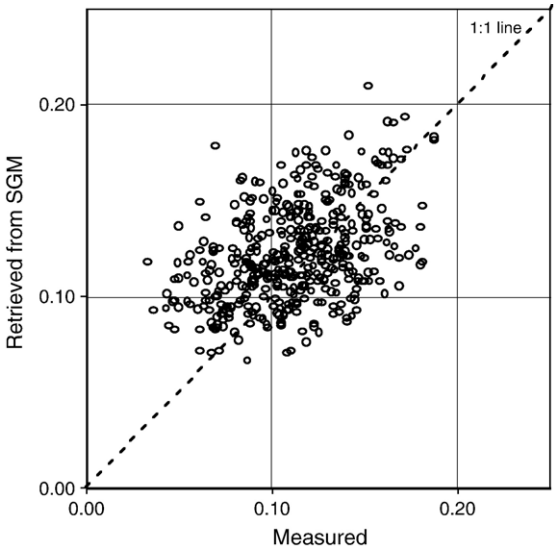

Fig. 15. Fractional shrub cover retrieved *via* inversion of SGM *vs* measured shrub cover from IKONOS panchromatic imagery. N=441, RMSE=0.03, r^2=0.19.

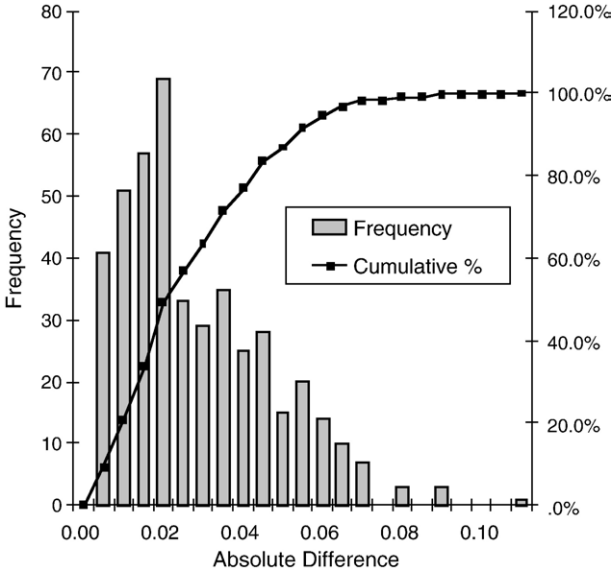

Fig. 16. Absolute difference in retrieved *vs* measured fractional shrub cover for a 21×21×250 m area in Chihuahuan Desert grassland in the Jornada Experimental Range.

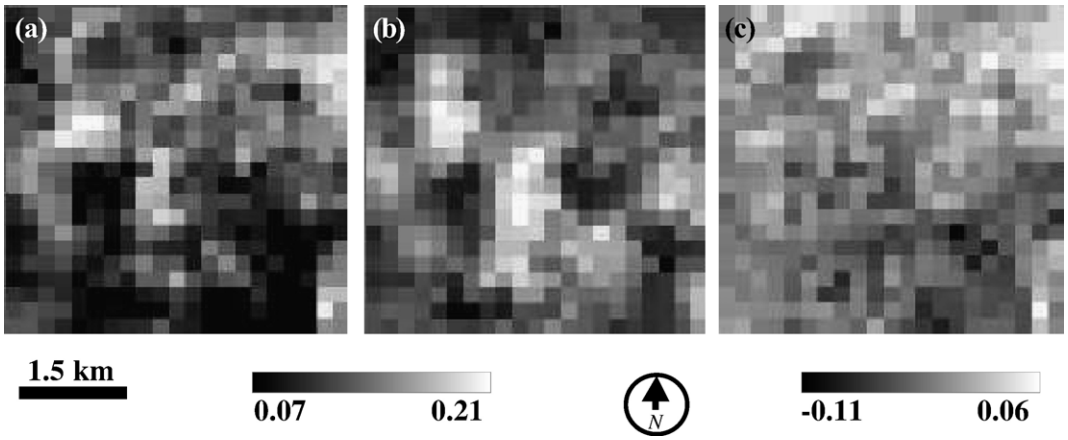

Fig. 17. Maps of fractional shrub cover scaled between 0.07 and 0.21 for a 21 × 21 × 250 m area. (a) derived from IKONOS (b) retrieved from MISR through inversion of the SGM (c) measured minus retrieved, scaled between −0.11 and +0.06.

0.012 (750 plants/250 m^2), 0.2 and 2.0, respectively, using numerical methods and using min(absolute RMSE) as the merit function. Since shrub radius and number density are internally coupled in the model, it is not feasible to estimate shrub cover without injecting *a priori* information. The flowchart in Fig. 11 provides an overview of the approach.

3. Results and discussion

The MISR reflectance simulations with SGM showed a good agreement with the MISR data, with an r^2 of 0.78 and RMSE of 0.013 for N=3969 (9 views × 441 locations) (Fig. 12). This compares well with previous attempts using only a single metric (volume scattering) to predict the background, which provided a maximum r^2 of 0.12 and higher RMSE values. The r^2 by camera (Df through Da) were 0.37, 0.42, 0.52, 0.48, 0.44, 0.47, 0.46, 0.38, and 0.29; the respective absolute RMSE values were 0.014, 0.012, 0.010, 0.014, 0.009, 0.010, 0.011, 0.013, and 0.018, implying a somewhat greater difficulty in modeling reflectance at more severe view zenith angles. The spatial distributions of the simulated multi-angle images differ somewhat from the MISR images (Fig. 13); they are somewhat noisy and the difference is particularly marked in the NE section where modeled shrub cover is lower than that estimated from IKONOS imagery. These differences reflect both the imperfect estimation of the soil-understory background BRDF at the Sun-target-MISR angular configurations as well as uncertainty in the IKONOS estimates; note too that the simulated images shown cover the MISR extreme forward, near-nadir and extreme aft views. This may partly be owing to the lag between the MISR and IKONOS acquisitions, although conditions will not have changed dramatically during this drought period. Profiles extracted from the simulated MISR images show that even where the understory is dense the contributions of the background and upper canopy are reasonable (Fig. 14).

Fractional shrub cover values for all 441 locations obtained by adjusting the SGM against the MISR data resulted in a RMSE of 0.03 and an r^2 of 0.19 with respect to measured values (Fig. 15). Estimation error is normally distributed and in terms of absolute deviation from the true value, about 90% of modeled values were within 0.05 of the true value (Fig. 16), although this is qualified by recognizing that variation in cover is low. The spatial distribution of retrieved shrub cover shows a good match except for a part of the NE quadrant where retrieved cover was too low; and a part of the SE quadrant where retrieved cover was too high (Fig. 17).

4. Conclusions

This study describes a new approach to applying geometric-optical models for shrub cover mapping in desert grasslands using moderate resolution multi-angle remote sensing data. This is achieved by partially isolating the soil-understory background signal from the combined upper canopy/background signal using MISR-derived Li–Ross model kernel weights and nadir spectral data. To our knowledge this is the first time that such an approach has been followed. Estimates of volume scattering were shown to be important — in addition to brightness from nadir green band BRFs and red isotropic kernel weights — in obtaining a spatially dynamic background. The use of MISR with a kernel-driven model is important in this application as the consistent angular sampling is necessary in order to obtain spatially consistent volume scattering maps; volume scattering estimates are invariably noisy if the angular sampling is inconsistent. The method was tested in a landscape scale study area of 5.25 km^2 in the USDA, ARS Jornada Experimental Range encompassing a wide range of canopy conditions. Single metrics (volume scattering kernel weights and diffuse brightness) were inadequate for predicting the soil-understory background signal. Multi-angle red wavelength images at MISR acquisition angles simulated using this approach were in good agreement with observed MISR sequences for all nine MISR cameras and for a wide range of canopy/background configurations, including shrubs within an area with a very dense understory of grasses, forbs, annuals, and sub-shrubs. Inversion of the SGM using numerical methods provided a map of fractional shrub cover in which the spatial distribution mostly matches that from high resolution panchromatic imagery and which provided an overall RMSE of 0.03.

To our knowledge this is the first time that moderate resolution satellite remote sensing data and a GO model have been used to

obtain a spatially extensive map of woody shrub cover in desert grasslands and in spite of some discrepancies, 90% of the fractional shrub cover estimates were within 0.05 of the true value for a wide range of canopy configurations and understory densities, within the range of shrub cover values in this landscape area (0.03 to 0.19). It is important to note that although the overall correlation between estimates from the high resolution and moderate resolution data is rather low, the good spatial match in the distribution of retrieved shrub cover implies that such model inversion efforts may provide useful measures of woody plant fractional cover over large areas where the range of cover values will vary over a wider domain. However, this may require recalibration of the relationships between the kernel weights and the background; furthermore, the disparities between simulated and observed MISR multi-angle images highlight the need for further research to determine how error is partitioned between uncertainties in the shrub statistics extracted from the high resolution IKONOS imagery and the model.

Acknowledgements

We thank Diane E. Wickland, Garik Gutman, and David J. Diner for their kind support and encouragement. This work was supported by NASA EOS Grant NNG04GK91G to the first author.

References

Asner, G. P., Borghi, C., & Ojeda, R. (2003). Desertification in Central Argentina: Regional changes in ecosystem carbon-nitrogen from imaging spectroscopy. *Ecological Applications*, *13*, 629−648.

Bahre, C. J., & Shelton, M. L. (1993). Historic vegetation change, mesquite increases, and climate in southeastern Arizona. *Journal of Biogeography*, *20*(5), 489−504.

Buffington, L. C., & Herbel, C. H. (1965). Vegetational changes on a semidesert grassland range from 1858 to 1963. *Ecological Monographs*, *35*(2), 139−164.

Calvão, T., & Palmeirim, J. M. (2004). Mapping Mediterranean scrub with satellite imagery: Biomass estimation and spectral behaviour. *International Journal of Remote Sensing*, *25*(16), 3113−3126.

Chopping, M. J. (2000). Large-scale BRDF retrieval over New Mexico with a multiangular NOAA AVHRR data set. *Remote Sensing of Environment*, *74*(1), 163−191.

Chopping, M. J., Su, L., Rango, A., & Maxwell, C. (2004). Modelling the reflectance anisotropy of Chihuahuan Desert grass–shrub transition canopy–soil complexes. *International Journal of Remote Sensing*, *25*(14), 2725−2745.

Chopping, M., Laliberte, A., & Rango, A. (2004). Exploitation of multi-angle data from CHRIS on Proba: First results from the Jornada Experimental Range. *Proceedings of the 2nd European Space Agency Workshop on CHRIS/Proba, April 28–30, 2004, ESRIN, Frascati, Italy, ESA Special Publication SP-578*. ISBN No: 92-9092-889-1. Compiled by: H. Lacoste.

Chopping, M., Laliberte, A., Rango, A., Snyder, C., & Maxwell, C. (2004, September 20–24). Differences in grass–shrub transition zone canopy composition from CHRIS/Proba multi-angle data, F17 — Multi-angular optical measurements. *Proc. International Geoscience and Remote Sensing Symposium 2004 VII: 4746–4749.* Alaska: Anchorage.

Chopping, M., Laliberte, A., & Rango, A. (2004, September 20–24). Multi-Angle data from CHRIS/Proba for determination of canopy structure in desert rangelands. F17 — Multi-angular optical measurements. *Proc. International Geoscience and Remote Sensing Symposium 2004 VII: 4742–4745.* Alaska: Anchorage.

Chopping, M. J., Rango, A., Havstad, K. M., Schiebe, F. R., Ritchie, J. C., Schmugge, T. J., et al. (2003). Canopy attributes of Chihuahuan Desert grassland and transition communities derived from multi-angular airborne imagery. *Remote Sensing of Environment*, *85*(3), 339−354.

Diner, D. J., Beckert, J. C., Reilly, T. H., Bruegge, C. J., Conel, J. E., Kahn, R. A., et al. (1998). Multi-angle Imaging SpectroRadiometer (MISR) instrument description and experiment overview. *IEEE Transactions on Geoscience and Remote Sensing*, *36*(4), 1072−1087.

Franklin, J., & Turner, D. L. (1992). The application of a geometric optical canopy reflectance model to semiarid shrub vegetation. *IEEE Transactions on Geoscience and Remote Sensing*, *30*(2), 293−301.

Gemmell, F. (2000). Testing the utility of multi-angle spectral data for reducing the effects of background spectral variations in forest reflectance model inversion. *Remote Sensing of Environment*, *72*, 46−63.

Gibbens, R. P, McNeely, R. P., Havstad, K. M., Beck, R. F., & Nolen, B. (2005). Vegetation changes in the Jornada Basin from 1858 to 1998. *Journal of Arid Environments*, *61*, 651−668.

Gillette, D. A., & Pitchford, A. M. (2004). Sand flux in the northern Chihuahuan desert, New Mexico, USA, and the influence of mesquite-dominated landscapes. *Journal of Geophysical Research*, *109*.

Grover, H. D., & Brad Musick, H. B. (1990). Shrubland encroachment in southern New Mexico, U.S.A.: An analysis of desertification processes in the American southwest. *Climatic Change*, *17*(2–3), 305−330.

Harrison, S. P., Kohfeld, K. E., Roelandt, C., & Claquin, T. (2001). The role of dust in climate changes today, at the last glacial maximum and in the future. *Earth Science Reviews*, *54*(1), 43−80.

Hu, B., Lucht, W., Li, X., & Strahler, A. H. (1997). Validation of kernel-driven models for global modeling of bidirectional reflectance. *Remote Sensing of Environment*, *62*, 201−214.

Huete, A. R. (1988). A soil-adjusted vegetation index. *Remote Sensing of Environment*, *25*, 295−309.

Laliberte, A. S., Rango, A., Havstad, K. M., Paris, J. F., Beck, R. F., McNeely, R., et al. (2004). Object-oriented image analysis for mapping shrub encroachment from 1937 to 2003 in southern New Mexico. *Remote Sensing of Environment*, *93*, 198−210.

Li, X., & Strahler, A. H. (1992). Geometric-optical bidirectional reflectance modeling of the discrete crown vegetation canopy: Effect of crown shape and mutual shadowing. *IEEE Transactions on Geoscience and Remote Sensing*, *30*(2), 276−291.

Lucht, W., & Lewis, P. (2000). Theoretical noise sensitivity of BRDF and albedo retrieval from the EOS-MODIS and MISR sensors with respect to angular sampling. *International Journal of Remote Sensing*, *21*, 81−98.

Ni, W., & Li, X. (2000). A coupled vegetation–soil bidirectional reflectance model for a semi-arid landscape. *Remote Sensing of Environment*, *74*(1), 113−124.

Okin, G. S., Roberts, D. A., Murray, B., & Okin, W. J. (2001). Practical limits on hyperspectral vegetation discrimination in arid and semiarid environments. *Remote Sensing of Environment*, *77*, 212−225.

Peddle, D. R., Franklin, S. E., Johnson, R. L., Lavigne, M. B., & Wulder, M. A. (2003). Structural change detection in a disturbed conifer forest using a geometric optical reflectance model in multiple-forward mode. *IEEE Transactions on Geoscience and Remote Sensing*, *41*(1), 163−166.

Peters, D. P. C., & Gibbens, R. P. (2006). Plant communities in the Jornada Basin: The dynamic landscape. In K. Havstad, L. Huenneke, & W. Schlesinger (Eds.), *Structure and Function of a Chihuahuan Desert ecosystem: The Jornada Basin Long-Term Ecological Research Site.* Oxford: OUP, 465 pp.

Peters, D. P. C., Schlesinger, W. H., Herrick, J. E., Huenneke, L. F., & Havstad, K. M. (2006). Future directions in Jornada research: Applying an interactive landscape model to solve problems. In K. Havstad, L. Huenneke, & W. Schlesinger (Eds.), *Structure and Function of a Chihuahuan Desert ecosystem: The Jornada Basin Long-Term Ecological Research Site.* Oxford: OUP, 465 pp.

Phinn, S., Franklin, J., Hope, A., Stow, D., & Huenneke, L. (1996). Biomass distribution mapping using airborne digital video imagery and spatial statistics in a semi-arid environment. *Journal of Environmental Management*, *47*(2), 139−164.

Pinty, B., Widlowski, J. -L., Gobron, N., Verstraete, M. M., & Diner, D. J. (2002). Uniqueness of multiangular measurements: Part 1. An indicator of subpixel surface heterogeneity from MISR. *IEEE Transactions on Geoscience and Remote Sensing*, *40*(7), 1560−1573.

Qi, J., Chehbouni, A., Huete, A. R., Kerr, Y. H., & Sorooshian, S. (1994). A modified soil adjusted vegetation index. *Remote Sensing of Environment*, *48*, 119−126.

Qin, W., & Gerstl, S. A. W. (2000). 3-D scene modeling of Jornada semi-desert vegetation cover and its radiation regime. *Remote Sensing of Environment*, *74*, 145−162.

Ray, T. W. (1995), Remote Monitoring of Land Degradation in Arid/Semiarid Regions, unpublished PhD Thesis, California Institute of Technology, 391 pp.

Ross, J. K. (1981). *The radiation regime and architecture of plant stands.* The Hague: Dr. W. Junk Publishers, 392 pp.

Scarth, P., & Phinn, S. (2000). Determining forest structural attributes using an inverted geometric-optical model in mixed Eucalypt forests, Southeast Queensland, Australia. *Remote Sensing of Environment*, *71*(2), 141−157.

Schaaf, C., Strahler, A., Liu, J., Salomon, J., Jiao, Z., Shuai, Y., et al. (2005). Reprocessed Aqua/Terra MODIS BRDF/Albedo product for use in modeling studies. *9th International Symposium on Physical Measurements and Signature in Remote Sensing (ISPMSRS), Beijing, China, Oct. 17–19*, *vol. I* (pp. 176−177).

Schlesinger, W. H., Reynolds, J. F., Cunningham, G. L., Huenneke, L. F., Jarrell, W. M., Virginia, R. A., et al. (1990). Biological feedbacks in global desertification. *Science*, *247*, 1043−1048.

Walthall, C. L., Norman, J. M., Welles, Campbell, G., & Blad, B. L. (1985). Simple equation to approximate the bidirectional reflectance from vegetative canopies and bare surfaces. *Applied Optics*, *24*, 383−387.

Wanner, W., Li, X., & Strahler, A. H. (1995). On the derivation of kernels for kernel-driven models of bidirectional reflectance. *Journal of Geophysical Research*, *100*, 21,077−21,090.

White, M. A., Asner, G. P., Nemani, R. R., Privette, J. L., & Running, S. W. (2000). Measuring fractional cover and leaf area index in arid ecosystems–digital camera, radiation transmittance, and laser altimetry methods. *Remote Sensing of Environment*, *74*(1), 45−57.